Yttrium and zirconium sorption on iron tin functionalized with silica: preparation, characterization, isotherm, and kinetic modelling

Sara S. Mahrous[1] · R. A. Abou-Lilah[2] · M. R. Abass[2]

Abstract

The sorption of Zr(IV) and Y(III) was examined using an iron-tin silicate (FeSnSi) composite prepared by the co-precipitation technique. The analytical tools that characterize prepared composite are FT-IR, SEM, EDX, XRD, and XRF. The effects of temperature, pH, ion concentrations, and shaking time are all considered in the sorption studies conducted on Zr(IV) and Y(III). The sorption of studied metal ions depends on pH, and the pseudo-2nd-order model governs the kinetics of reactions. Negative Gibbs energy values confirmed the excellent feasibility and spontaneity of the sorption process. Positive enthalpy values indicate that this process was endothermic. Positive entropy values demonstrated that the disorder between the solid and liquid phases was enhanced during adsorption. Freundlich and Langmuir models are used to study isotherms. The results of the binary system verify that Zr(IV) may be separated from the Zr-Y system at various pHs. According to the findings, the produced composite may effectively remove Zr(IV) and Y(III) from aqueous solutions. It may also be viable for purifying wastewater contaminated with these metal ions.

Keywords Zr(IV) · Y(III) · FeSnSi · Reaction kinetic · Thermodynamic · Binary system

1 Introduction

Rare earth elements (REEs) comprise 15 lanthanides and two pseudo-lanthanides (scandium and yttrium). These elements can be further classified into light rare earth elements (LREEs) and heavy rare earth elements (HREEs). The LREEs are La, Ce, Pr, Nd, Pm, Eu, Gd, and Sm. The list of HREEs is Dy, Y, Tb, Ho, Er, Tm, Yb, and Lu. REEs, are sometimes known as the "industrial vitamin," because they play critical roles in the development of worldwide sustainable energy technologies [1, 2]. The combination of five crucial REEs (Dy, Eu, Nd, Tb, and Y) collectively accounts for as much as 63% of the overall weight of all REEs in the final product, with a purity of 99.4%. Yttrium is extensively utilized in several industries for its exceptional physicochemical qualities, serving as catalysts,

sensors, fiber optics, and flattened screen displays [3, 4]. Moreover, yttrium is commonly utilized in the field of medicine for purposes such as tumor therapy, food irradiation methods, and sewage treatment procedures. One of the most frequent radioisotopes found in liquid radioactive waste due to the fission reaction is ^{90}Sr. It undergoes decay with a half-life of 28 years by emitting electrons (beta minus decay) and transforms into ^{90}Y. Some recent investigations have found that long-term yttrium exposure in humans can result in carcinoma of the lungs, and damaged liver function [5–8]. Recovering yttrium from wastewater not only reduces the ecological and health hazards linked to yttrium-contaminated aquatic ecosystems but also contributes to fulfilling the increasing worldwide need for yttrium [9].

Zirconium is employed in nuclear power plant technology as a cladding material in the form of zircalloys for uranium fuel and other components within the reactor. The deterioration of reactor vessels due to aging results in erosion, which in turn leads to the contamination of coolant water with radioactive zirconium species, hence creating risks to the ecosystem [10]. Zirconium and its derivatives have extensive applications in several industries such as the chemical industry, steel and cast production, satellite surface agents, lamp filaments, welding fluxes, vacuum tubes, water-resistant textiles, dye pigments, ceramics, glass, and abrasives. Therefore, it is

✉ M. R. Abass
mohamed.ragab2014300@yahoo.com

1 Environmental Radioactive Pollution Department, Hot Laboratories and Waste Management Center, Egyptian Atomic Energy Authority, Cairo 13759, Egypt

2 Nuclear Fuel Technology Department, Hot Laboratories and Waste Management Center, Egyptian Atomic Energy Authority, Cairo, Egypt

crucial to purify the coolant water in the reactor by removing radioactive zirconium and other generated radioactive waste before it can be safely discharge in the environment [10, 11].

Wastewater contaminated with hazardous metal ions has been treated using a variety of techniques, such as chemical precipitation, membrane separation, electrodeposition, ion exchange, solvent extraction, and adsorption [12, 13]. The most economical of these techniques are traditional chemical precipitation, however, it is ineffective for diluted solutions. Reverse osmosis and ion exchange are generally efficient, however, they have relatively significant operational and maintenance expenses. One of the few viable choices for this application is adsorption, due to its cost-effective and simple handling. Furthermore, one of the most important features of the adsorption technique is the possibility of separating one or several similar elements from the mixed solution and quantitatively determining [14]. Silica gels are a beneficial material used as a pre-concentration surface for a variety of compounds, including metals from aquatic systems. Matrix that can host a wide range of components can be created by chemically modifying silica gels with organic or inorganic molecules or both, these matrices have vast technological applications. Wastewater treatment is reliably enhanced by these cutting-edge materials, which are both environmentally safe and highly effective [14].

Many studies have been carried out for the sorption of Y(III) and Zr(IV) using different sorbent materials [15–20], but FeSnSi composite has not been used previously for the removal of Y(III) and Zr(IV). In this work, FeSnSi composite was prepared as novel material and used for the sorption of Y(III) and Zr(IV) from aqueous solutions. This sorbent material is prepared by incorporating iron chloride and stannous chloride into the silica matrix. The synthesized sorbent was characterized using different analytical tools. This composite was tested under various batch experimental circumstances to see if it could be used to solid-phase extract Zr(IV) and Y(III) from their respective aqueous solutions.

2 Experimental

2.1 Materials and instruments

The main reagents used were YCl_3, HNO_3, and HCl (Merck, Germany). $FeCl_3.6H_2O$ (Loba Chemie, India), $SnCl_2.2H_2O$, $ZrOCl_2$, and Na_2SiO_3 (Alpha Chemika, India), as well as NaOH and NH_3 (El-Nasr Co, Egypt). The compounds and components used in this article are of analytical quality, meaning they do not require any additional purification. Double distilled water (DDW) was used for all experiments involving the preparation of composites and solutions. We used an Alpha II Bruker from Germany for Fourier-transform infrared spectroscopy (FT-IR) and a Brucker XRD diffractometer D2 Phaser II from Germany for X-ray diffraction (XRD) analysis of the FeSnSi composite. We used a Philips sequential X-ray spectrometer-2400 to determine the FeSnSi composite's elemental composition. The Super-Q quantitative application program dictated SiO_2, Fe_2O_3, and SnO_2 percentages. The morphology and elemental analysis of the FeSnSi composite were examined using scanning electron microscopy (SEM) and energy-dispersive X-ray (EDX) analysis model (ZEISS—EVO 15, UK).

2.2 Preparation

2.2.1 Preparation of reagents

Using 600 mL of DDW and 60 g of Na_2SiO_3 powder, a 10% (w/v) solution was made by mixing them for 60 min. After dissolving 4.866 g of $FeCl_3$ powder in 150 mL of DDW for 1 h, a 0.2 M solution of $FeCl_3$ was obtained. 17.79 g of $SnCl_2.2H_2O$ powder was dissolved in 300 mL of 4 M HCl for 2 h to produce a $SnCl_2.2H_2O$ solution (0.2 M).

2.2.2 Preparation of iron tin silicate (FeSnSi) composite

The SnSi and FeSnSi composites were prepared using a co-precipitation technique. In this method, $FeCl_3$ solution (0.2 M) and $SnCl_2.2H_2O$ solution (0.2 M) were dropwise to Na_2SiO_3 solution by various volumetric ratios at constant stirring as shown in Table 1. The reaction mixture was diluted to one litter and let to settle for one day after total addition, which produced a brownish-red tint. Subsequently, NH_4OH (10% v/v) was added dropwise to the combined solution until a precipitate formed at pH 7.2. Precipitate washed several times to remove free chloride ions. Drying the precipitate at 55 ± 1 °C for 24 h followed by grinding and sieving it for different mesh sizes was followed by storage at 25 ± 1 °C.

Table 1 Conditions for the synthesis of different composites and their % R of Zr(IV) and Y(III) [50 mg L^{-1}, V/m = 100 mL g^{-1}, and shaking time 24 h] at room temperature

Samples	Composites	$FeCl_3.6H_2O$, (0.2 M)	$SnCl_2.2H_2O$, (0.2 M)	Na_2SiO_3, (10% w/v)	% Removal	
					Zr(IV)	Y(III)
1	SnSi	–	100	200	63.5	45.4
2	FeSnSi	50	100	200	79.9	64.0
3	FeSnSi	100	100	200	96.8	84.1

2.3 The percent removal studies

To select the optimal sample for percent removal (% R), SnSi and FeSnSi composites were made using various volumetric ratios of Zr(IV) and Y(III) (50 mg L^{-1}) and agitated with 0.05 g solid, 5 mL of Zr(IV) and Y(III) (V/m = 100 mL g^{-1}), at 30 ± 1˚C for 24 h. At this point, the agitator is turned off, then solid and solution are immediately separated. UV–visible recording spectrophotometer (UV-160A) made and supplied by Shimadzu Kyoto, Japan, was utilized to measure the initial and final concentrations (C$_i$ and C$_f$) of Y(III) and Zr(IV). Using (Eq. (1)), one may get the % R [21, 22]:

$$\% \, R = \left(\frac{C_i - C_f}{C_i} \right) 100 \tag{1}$$

The data shown in Table 1 demonstrates the % R of Zr(IV) and Y(III) onto SnSi and FeSnSi composites, which were prepared using various volumetric ratios. The results indicate that Zr(IV) removal is more than Y(III) removal, and sample 3 (S-3) exhibits the highest efficiency. Consequently, it was selected for this study based on its higher percentage of elimination.

2.4 pH titration

Topp and Pepper's method was used to study the pH titration of FeSnSi composite utilizing the NaOH-NaCl system [23]. Each NaOH-NaCl system was supplemented with 0.1 g of solid powder and subjected to continuous shaking in 10 mL volumes. The pH of the solution was measured using a laboratory pH meter at regular one-day intervals until it achieved equilibrium.

2.5 Chemical stability

The chemical stability of S-3 was assessed by subjecting 0.2 g of solid and 20 mL of various solvents, including mineral acids, and alkaline solution to agitation for approximately 3 days at a temperature of 25 ± 1 °C. The quantity of S-3 discharged into the solution was measured by gravimetric analysis [21, 22].

2.6 Sorption investigations

The ideal conditions for sorption are determined by carefully examining many parameters, including pH levels ranging from 0.5 to 5, batch factor V/m values ranging from 50 to 1000 mL g^{-1}, reaction temperatures of 298, 308, 318, 328, and 338 K, metal ion concentrations ranging from 25 to 600 mg L^{-1}, and agitation times ranging from 2 to 180 min. The sorbent and sorbate solution were brought into contact

using a batch process. After sorption occurred, the samples were removed from the solution using filtration. The equilibrium measurements were conducted by agitating 0.05 g of S-3 with 5 mL of Zr(IV) and Y(III) solutions, which had an initial concentration of 50 mg L^{-1}, using an agitator thermostat (Kottermann D-1362, Germany) at a volume-to-mass ratio of 100 mL g^{-1}. In this inquiry, all the recorded experimental data was obtained by averaging the results of two identical tests conducted in duplicate. The equilibrium adsorption capacity (q$_e$), mg g^{-1} of Zr(IV) and Y(III) on S-3 were obtained using the relevant formula [24–26]:

$$q_e = \left(\frac{C_i - C_e}{m} \right) V \tag{2}$$

where C$_e$ is the equilibrium concentration of Zr(IV) and Y(III), mg L^{-1}. V and m represent the volume of the effluent solution in liters and the amount of S-3 per gram, respectively.

2.7 Study of the rate of a chemical reaction

To elucidate the adsorption process, we will discuss the nonlinear form of the pseudo-1st-order equation (PFO) (Eq. (3)) and the pseudo-2nd-order equation (PSO) (Eq. (4)). The PFO model is a model of a system consisting of a solid and a liquid, which is based on the adsorption capacity of the adsorbent [27]. The PSO model relies on the quantity of active sites present on the adsorbent surface and the adsorption capacity of the solid phase [28].

$$q_t = q_e \left[1 - \exp(-K_1 t) \right] \tag{3}$$

$$q_t = \frac{q_e^2 K_2 t}{1 + q_e K_2 t} \tag{4}$$

q$_t$ and q$_e$ represent the quantity of substance adsorbed at time t and the quantity of substance adsorbed at equilibrium, mg g^{-1}, respectively. t represents the time in min, while K$_1$ and K$_2$ represent the rate constants of the PFO and PSO models, respectively. The rate constant of the PFO model is measured in minutes to the power of a negative one, while the rate constant of the PSO model is measured in grams per milligram per minute.

2.8 Impact of temperature

Thermodynamic calculations can be used to ascertain the spontaneity of the adsorption process. Moreover, by utilizing thermodynamic characteristics at various reaction temperatures (298, 308, 318, 328, and 338 K), we can demonstrate the impact of temperature on the sorption of Zr(IV) and Y(III) onto S-3. The thermodynamic parameters were determined by

studying the percentage of Zr(IV) and Y(III) sorption onto S-3 at pH 2.5 and 4 for Zr(IV) and Y(III). The equations employed for the determination of enthalpy ($\Delta H°$), entropy ($\Delta S°$), and Gibbs free energy ($\Delta G°$) are as follows: [29–31];

$$K_d = \left(\frac{C_i - C_f}{C_f} \right) \frac{V}{m} \tag{5}$$

$$\Delta G^o = -RT\ln(K_d) \tag{6}$$

$$\ln K_d = \frac{\Delta S^o}{R} - \frac{\Delta H^o}{RT} \tag{7}$$

$$\Delta G^o = \Delta H^o - T\Delta S^o \tag{8}$$

K_d represents the distribution coefficient, mL g^{-1}.

2.9 Modelling of isotherms

The concentration data acquired for the determination of the isotherms of Zr(IV) and Y(III) loaded onto FeSnSi were examined using a non-linear version of the Langmuir Eqs. (9&10) and the Freundlich Eq. (11). Sorption isotherms were conducted at pH 4 and 2.5 for Y(III) and Zr(IV), respectively, with initial concentrations ranging from 25 to 600 mg L^{-1}. According to the Langmuir model, the adsorbent surface has active centers of adsorption that are evenly distributed [32]. The Freundlich model elucidates the hyperbolic adsorption behavior and offers insights into the heterogeneity of the adsorbent surface [33].

$$q_e = q_m \frac{K_L C_e}{1 + K_L C_e} \tag{9}$$

$$R_L = \frac{1}{1 + K_L C_i} \tag{10}$$

$$q_e = K_F C_e^{\frac{1}{n}} \tag{11}$$

q_m, R_L, and K_L represent the maximum sorption capacity, mg g^{-1}, the dimensionless constant of separation factor, and the parameters for the Langmuir isotherm, respectively. K_F and $1/n$ represent the Freundlich constant and the degree of adsorbent surface heterogeneity, respectively.

2.10 Binary system

This study focuses on a binary system consisting of Zr and Y. A solution containing 5 mL of Zr-Y combination with an initial concentration of 50 mg L^{-1} is used. The ratio of solution volume to mass is 100 mL g^{-1}. The contact time is set at 90 min, and the initial pH ranges from 1 to 3. The separation factors (α_Y^{Zr}) were determined by evaluating the equation as a function of pH [24, 34]:

$$\alpha_Y^{Zr} = \frac{K_d Zr}{K_d Y} \tag{12}$$

3 Results and Discussion

3.1 X-ray diffraction analysis

The semi-crystalline nature of FeSnSi was observed from X-ray diffraction (XRD) as shown in Fig. 1a. The broad peak centered at 2θ from 9° to 26° is a known typical characteristic of amorphous silica [35, 36]. Sharp peaks at 2θ ≈ 32°and 45.4° characteristics to Fe_2O_3 and SnO_2 respectively [37–39].

Fig. 1 **a** XRD analysis and **b** FT-IR spectrum for FeSnSi composite
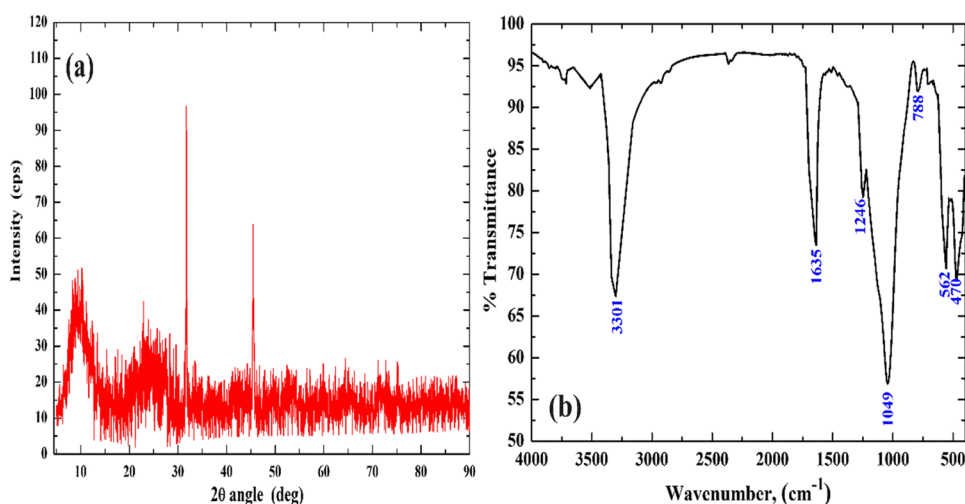
3.2 FT-IR analysis

The FT-IR spectrum of the FeSnSi composite in Fig. 1b shows two bands at 3301 and 1635 cm^{-1}. These bands correspond to the stretching and bending vibrations of the OH frequencies of water molecules within the composite structure, respectively [40]. The presence of a band at 1246 cm^{-1} indicates that there is a connection between Sn–O and an OH group, specifically in the form of a bending vibration. This band serves as evidence that Sn has been incorporated within a layer of FeSnSi, as demonstrated by the subsequent XRF results [41]. The band at 1049 is due to the metal–oxygen bond (Si–O-Si) [42]. The band at 788 cm^{-1} possibly results from Si–O bonding and is classified as a silicate group (SiO$_3$) [43, 44]. Bands at 562 and 470 cm^{-1} are attributed to metal oxide bonds (Fe–O and Sn–O), respectively [45].

3.3 XRF analysis

The elemental composition of the FeSnSi composite can be determined using XRF analysis and is presented in Table 2. These results confirm that the % of metals present in the FeSnSi composite is 85.86, 3.92, and 6.15 for SiO$_2$, Fe$_2$O$_3$, and SnO$_2$, respectively. As well as some traces such as Na$_2$O, SO$_3$, and MgO. The data has verified that the main components found in the FeSnSi composite are SiO$_2$, Fe$_2$O$_3$, and SnO$_2$.

3.4 Morphology analysis

The SEM and EDX analysis can be used to identify the morphological properties and surface elemental composition of the FeSnSi composite, as depicted in Fig. 2. Figure 2a illustrates the surface morphology of the FeSnSi composite indicating that the irregular surface and presence of different

Table 2 Elemental analysis of FeSnSi composite using X-ray fluorescence

Component	SiO$_2$	Fe$_2$O$_3$	SnO$_2$	Na$_2$O	SO$_3$	MgO
Concentration (%)	85.86	3.92	6.15	1.75	0.99	0.79

Fig. 2 **a** SEM image, **b** EDX, and **c** EDX mapping of FeSnSi composite
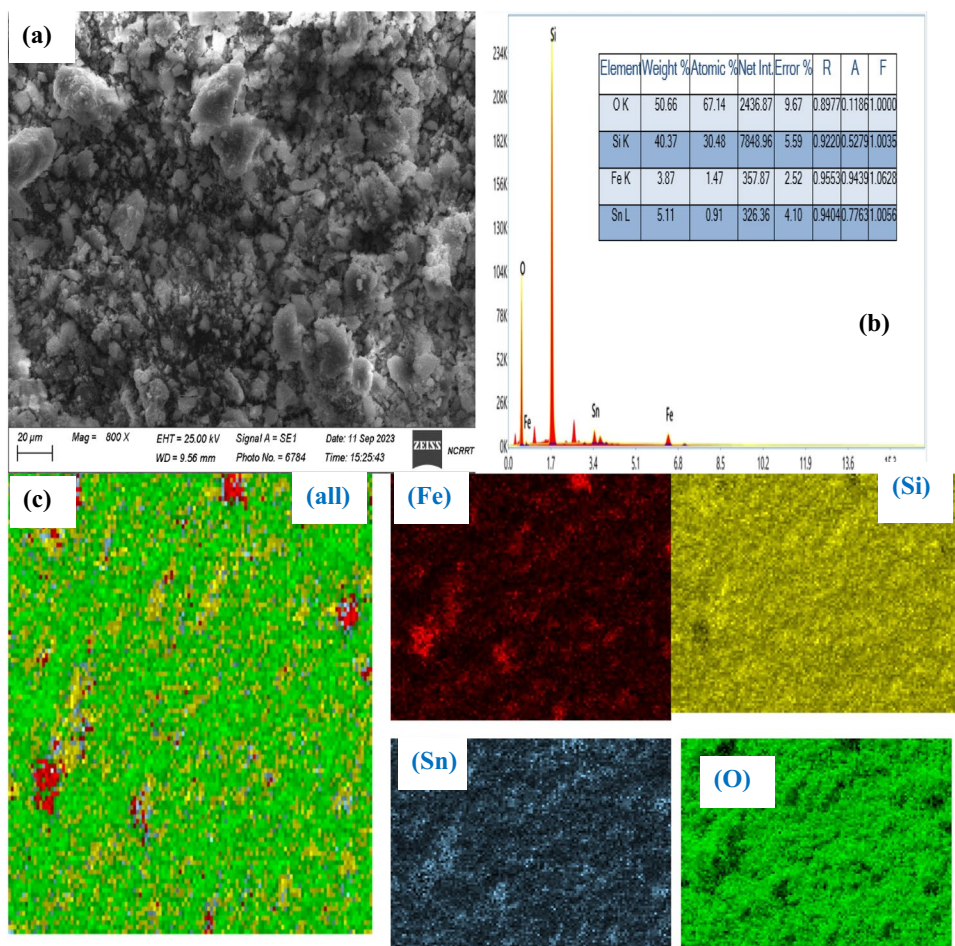
pores with different diameters confirmed the presence of different components. Multi-elemental EDX mapping images for FeSnSi composite signified the presence of O, Si, Sn, and Fe constituents as shown in Fig. 2b. EDX confirmed the presence of all atoms, with oxygen being the most prevalent ion at a mass percent of 50.6%. Silica, tin, and iron were also detected, accounting for 40%, 5%, and 3.9% respectively. Moreover, the maps corresponding to these peaks as shown in Fig. 2c revealed that there are bright spots with green, yellow, blue, and red colors with heterogeneous distribution for oxygen, silica, tin, and iron respectively in the view of the cross-section.

3.5 pH titration

Figure 3 illustrates the pH titration of the FeSnSi composite. The X-axis represents the amount of 0.1 M NaOH in millimoles per gram of FeSnSi composite, while the Y-axis shows the pH of the liquid that comes out. The pH titration of the FeSnSi composite has a single inflection point, indicating that the composite is monofunctionally. This chemical reaction has similarities to cerium(IV) molybdate [46] and SnSiMo [47].

3.6 Chemical stability

According to the results of the solubility test conducted on various solvents (Table 3), the FeSnSi composite exhibited remarkable stability when exposed to common mineral acids and alkalis. The chemical stability of the FeSnSi
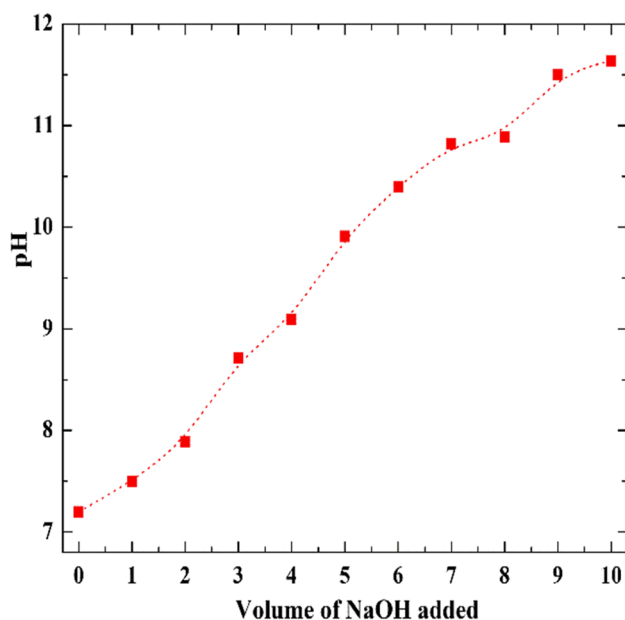
Table 3 Chemical stability of FeSnSi composite in different solvents

Solvents	Solubility, g L^{-1}
1 M HCl	0.1
2 M HCl	0.15
3 M HCl	0.21
4 M HCl	0.26
5 M HCl	0.29
1 M HNO$_3$	0.17
2 M HNO$_3$	0.23
3 M HNO$_3$	0.3
4 M HNO$_3$	0.35
5 M HNO$_3$	0.39
0.1 M KOH	0.06
1 M KOH	0.3
0.1 M NaOH	0.1
1 M NaOH	0.33

composite is comparatively high among alternative sorbents, as demonstrated in Table 3 [20, 39, 48].

3.7 Metal ions hydrolysis

The primary determinant of the separated elements by the suggested adsorbent is the metal hydrolysis side reaction, which is highly responsive to the pH of the solution. Regarding this, several examinations have been conducted autonomously. Thus, at various pH values ranging from 0.5 to 6, distinct samples (10 mL each) containing 50 mg L^{-1} of each element (in distilled water) were individually prepared. The samples were filtered following 30 min of agitation. Subsequently, the concentrations of each element at every pH value were determined using spectrophotometry to compute the precipitation percentage, as illustrated in Table 4. Before pH 5, Y(III) precipitated, and Zr(IV) precipitated at pH 3, respectively. To the outcomes of metal hydrolysis, the subsequent experiments were conducted at pH 2.5 and 4 for Zr(IV) and Y(III), respectively, to simulate acidic conditions and prevent the hydrolysis of the metal ions.

Fig. 3 pH titration curve of FeSnSi composite

Table 4 Metal hydrolysis (%) at different pH values

pH	Y(III)	pH	Zr(IV)
1	Nil	0.5	Nil
2.0	Nil	1.0	Nil
3.0	Nil	1.5	1.8
4.0	Nil	2.5	3.5
5.0	6.3	3.0	100
6.0	18.6	4.0	100

Fig. 4 Sorption of Y(III) and Zr(IV) onto FeSnSi composite, **a** Effect of pH on the % R, **b** Effect of shaking time on the % R, and **c** Effect of V/m on the % R
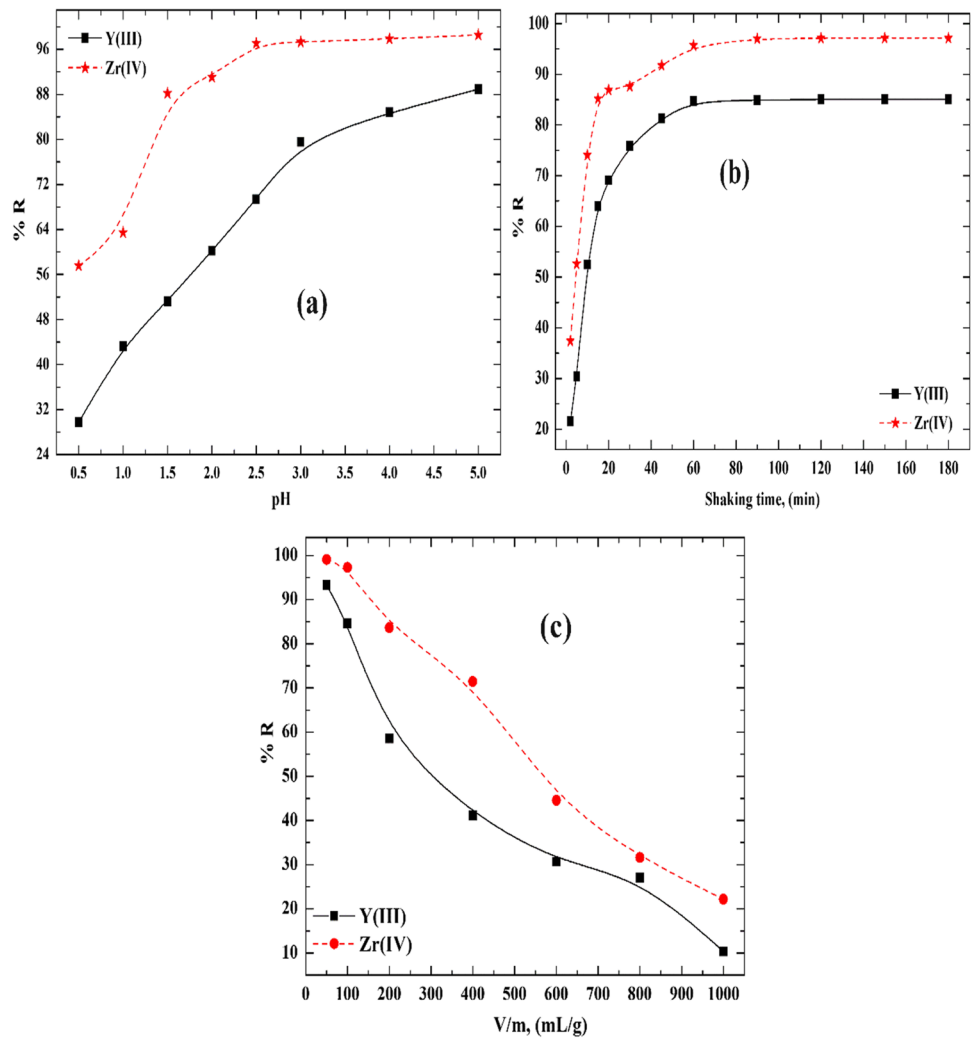

3.8 Impact of pH

The removal of Y(III) and Zr(IV) from aqueous solutions by the FeSnSi composite was studied as represented in Fig. 4a.

The % R rises with increasing pH (1–4) from 29.7% to 84.8% for Y(III) with the continuous increase at pH 5, (% R = 88.9% but this pH value Y(III) started to precipitate based on metal ion hydrolysis data mentioned in Table 4. The % R increases

Fig. 5 Kinetic modeling fitting of Y(III) and Zr(IV) onto FeSnSi composite at [$C_i = 50$ mg L^{-1}, V/m = 100 mL g^{-1}, pHs 4 and 2.5 for Y(III) and Zr(IV), respectively]
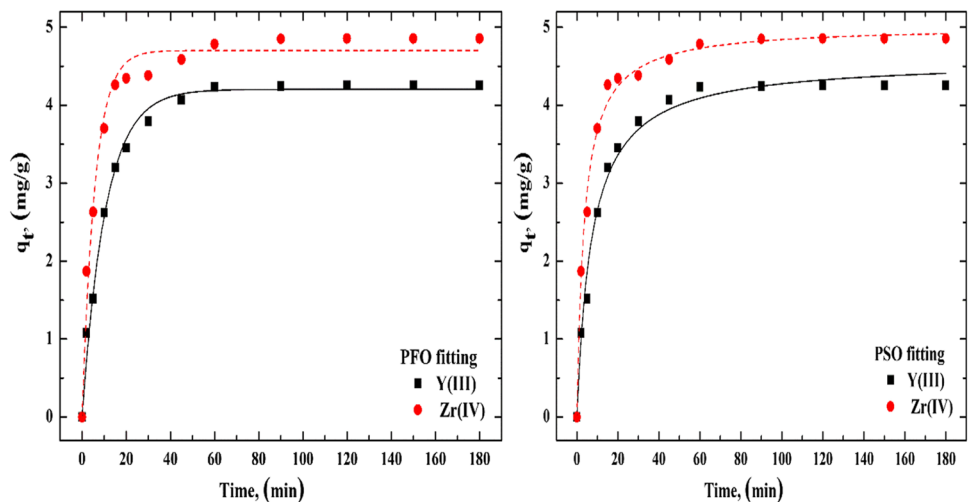
Table 5 Kinetic parameters and correlation coefficients (R^2) for the sorption of Y(III) and Zr(IV) onto FeSnSi composite

Metal ions	PFO		q_e (exp.)	PSO	
Y(III)	q_e(cal.)	4.20	4.24	q_e(cal.)	4.59
	K_1	0.094		K_2	0.030
	R^2	0.981		R^2	0.998
Zr(IV)	q_e(cal.)	4.70	4.85	q_e(cal.)	5.02
	K_1	0.172		K_2	0.054
	R^2	0.978		R^2	0.993

with increasing pH (0.5–2.5) from 57.6% to 97.3% for Zr(IV) with a slight increase of the % R with increasing of pH above this value due to the precipitation of Zr(IV) as mentioned in Table 4. All experimental procedures involving Y(III) and Zr(IV) were conducted at pH 4 and 2.5, respectively. Additionally, it was noted that the percentage R of Y(III) and Zr(IV) is diminished at low pH levels. This phenomenon can likely be attributed to the protonation of the surface-active sites and the accumulation of H_3O^+ ions in the aqueous solution. Thus, the competition between H_3O^+ and both Y(III) and Zr(IV) for the available binding surface active site was caused by the positively charged surface sites, which reduced Y(III) and Zr(IV) uptake. As the initial pH values increased, there was a concurrent decrease in the concentration of H_3O^+ ions and an increase in the concentration of OH^- ions. This phenomenon induces deprotonation at the sorbent surface. These findings indicate that the FeSnSi composite surface generally possesses a negative charge. As a result, an increase in attraction was observed between the positive charge of metal ions in the solution and the surface of the composite.

3.9 Impact of mixing time

At pH 4 and 2.5, the impact of contact time on the percent R of Y(III) and Zr(IV) on the FeSnSi composite was

investigated, respectively. As shown in Fig. 4b, the % R of Y(III) and Zr(IV) deposited onto the FeSnSi composite increases with time until it reaches equilibrium at approximately 90 min. The uptake rates of Y(III) and Zr(IV) onto the FeSnSi composite increase very rapidly from 2 to 60 min, then gradually from 60 to 90 min; beyond this time, there is no change in the uptake; therefore, 90 min was designated as the equilibrium time for subsequent experimental investigations.

3.10 Impact of batch factor (V/m)

Impact of V/m on % R of Y(III) and Zr(IV) onto the FeSnSi composite (Fig. 4c), was done at pH = 2.5 for Zr(IV) and 4 for Y(III). From this Figure, it is found that retention of Y(III) and Zr(IV) onto the FeSnSi composite highly reduced with rising the V/m ratio from (50–1000 mL g^{-1}) and V/m ratio (100 mL g^{-1}) was applied as a V/m to subsequent experimental procedures.

3.11 Kinetic study

To analyze the kinetics of adsorption, the experimental data were fitted with PFO and PSO model equations. Y(III) and Zr(IV) were adsorbed onto the FeSnSi composite in two distinct phases (Fig. 5). A phase of rapid adsorption transpired for a duration of 60 min during the initial stage. In contrast to the rapid and quantitatively dominant nature of the first stage, the second was markedly sluggish and quantitatively insignificant. Several active centers were readily accessible on the FeSnSi surface during the early stages of adsorption. The equilibrium state was attained once these centers were occupied; so, the second stage doesn't increase at a noticeable rate. Upon comparing the R^2 values of the PFO and PSO models (Table 5), it was determined that the

Fig. 6 Sorption of Y(III) and Zr(IV) onto FeSnSi composite, **a** Effect of reaction temperature on the % R and **b** Van't Hoff plot
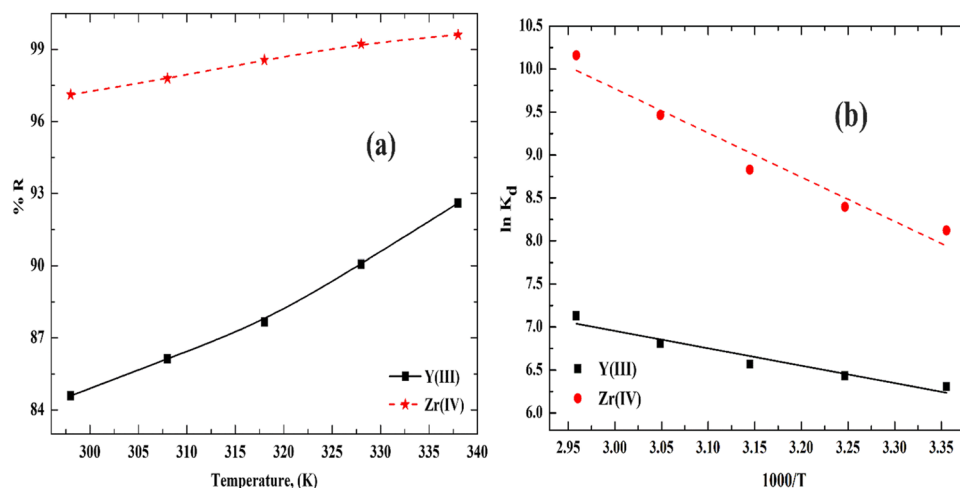
Fig. 7 Isotherm modelling fitting of Y(III) and Zr(IV) onto FeSnSi composite at [Eq. time = 90 min, V/m = 100 mL g^{-1}, pH 4 and 2.5 for Y(III) and Zr(IV), respectively]
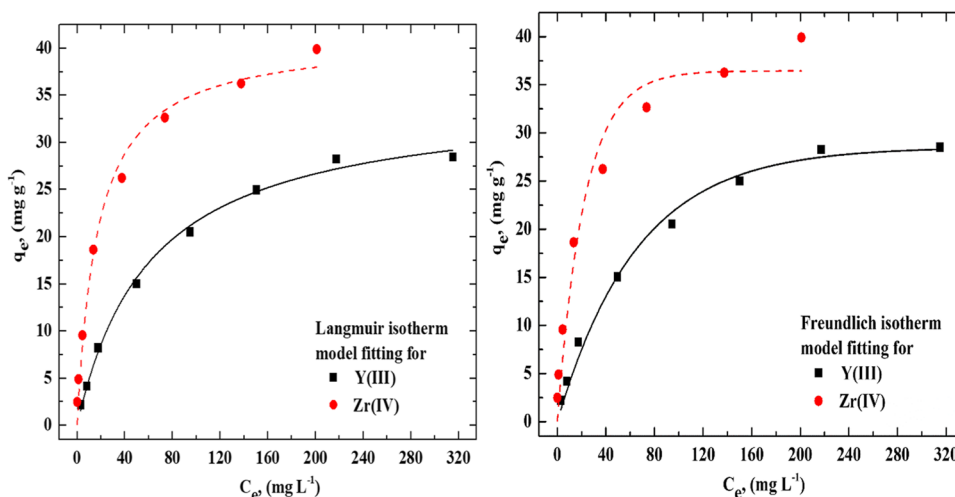
PSO provided a more accurate representation of the kinetics. Moreover, the experimental and theoretically determined q_e values were comparable, indicating that the PSO model was consistent. The obtained results indicate that the adsorption process adhered to the rate kinetics of PSO.

3.12 Studies on thermodynamics

The effect of reaction temperature on the % R of Y(III) and Zr(IV) onto FeSnSi composite was done at initial concentration of 50 mg L^{-1}, shaking time = 90 min, pH 4 and 2.5 for Y(III) and Zr(IV), respectively. The result is shown in Fig. 6a. This Figure shows how an increase in the % R of Y(III) and Zr(IV) with increasing reaction temperature reflects the endothermic nature of the sorption process. The thermodynamic behavior of the adsorption process was examined at temperatures of 298, 308, 318, 328, and 338 K (Fig. 6b). For Y(III) and Zr(IV) adsorption onto the FeSnSi composite, the change in $\Delta H°$ during the adsorption process was 16.8 and 42.8 kJ mol^{-1}, respectively. In the endothermic adsorption process, Y(III) and Zr(IV) sorption exhibited a favorable response to temperature increases. Furthermore, $\Delta S°$ was a 108.3 and 209.7 J mol^{-1} K^{-1} for Y(III) and Zr(IV), respectively. This result demonstrated the random nature of the adsorption process. Because of the high affinity of the adsorbent, a positive entropy could be interpreted as an increase in the randomness of the adsorption system [49]. At 298, 308, 318, 328, and 338 K, respectively, the free energy change for Y(III) was -15.4, -16.5, -17.6, -18.7, and

-19.8 kJ mol^{-1}, while for Zr(IV), it was -19.7, -21.8, -23.9, -26.0, and -28.1 kJ mol^{-1}. Negative values of $\Delta G°$ indicate that the adsorption process is spontaneous. In addition, the increase in temperature results in greater mobility of Y(III) and Zr(IV) on the surface of the FeSnSi composite. This leads to more significant electrostatic attraction between these cations and various active groups on the composite surface, which can be attributed to the higher values of $\Delta G°$ observed at higher temperatures.

3.13 Sorption isotherms

To find a suitable model for the design process, a variety of isotherm models were employed to examine the equilibrium data. The study utilized the Langmuir and Freundlich isotherm equations to examine the sorption of Zr(IV) and Y(III) onto the FeSnSi composite. Isotherm equations are consistently demonstrated to be applicable by the correlation coefficients (R^2). The interaction mechanism of FeSnSi with Y(III) and Zr(IV) at equilibrium was determined using adsorption isotherms. The comparison of R^2 values between the Freundlich isotherm and Langmuir isotherm models (Fig. 7, Table 6) indicates that the adsorption process of Y(III) and Zr(IV) conformed to the Langmuir isotherm, offering a better fit with $R^2 = 0.995$ and 0.983 for Y(III) and Zr(IV), respectively. The favorable sorption isotherms of Y(III) and Zr(IV) were found to be reflected in the R_L values of (0.092 and 0.028) [50]. The maximum sorption capacity was 34.8 and 41.3 mg g^{-1}, for Y(III) and Zr(IV),

Table 6 Isotherm parameters for sorption of Y(III) and Zr(IV) onto FeSnSi composite

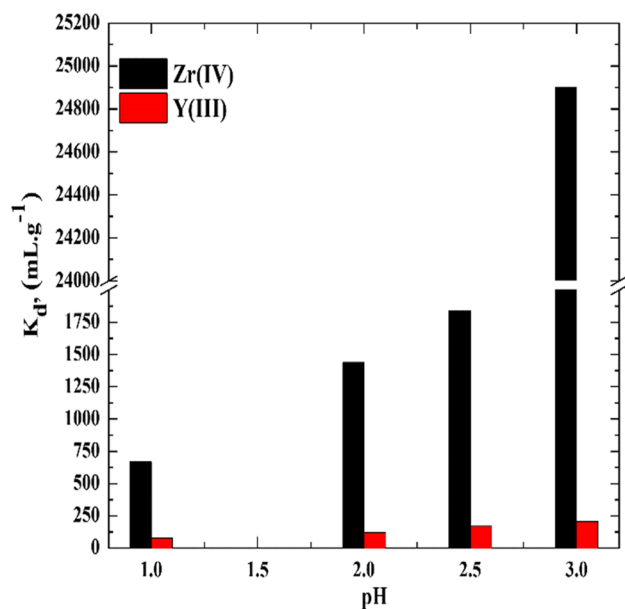| Metal ions	Langmuir			Freundlich		
	q_m	R_L	R^2	$1/n$	K_F	R^2
Y(III)	34.8	0.092	0.995	65.7	28.53	0.990
Zr(IV)	41.3	0.028	0.983	22.47	36.43	0.954

Table 7 Comparison of the maximum sorption capacity of Y(III) and Zr(IV) sorbed onto various composites

Composites	q_m, mg g^{-1}		Ref. no
	Y(III)	Zr(IV)	
FeSnSi	34.8	41.3	Current work
SDS-AZS	21.01	NR	[15]
PEI-GO-AG	38.17	NR	[16]
Natural clinoptilolite	NR	6.18	[17]
Bentonite	NR	48.56	[18]
Rice bran	NR	50.0	[19]

Table 8 Distribution coefficients and separation factors of Zr-Y binary system onto FeSnSi composite

pH	K_d and α_Y^{Zr}	Y(III)	Zr(IV)
1	K_d	79.21	666.87
	α_Y^{Zr}		8.42
2	K_d	121.93	1438.46
	α_Y^{Zr}		11.80
2.5	K_d	168.82	1837.98
	α_Y^{Zr}		10.89
3	K_d	208.64	24900.0
	α_Y^{Zr}		119.34

respectively. These findings verified that the Langmuir model fits the Y(III) and Zr(IV) adsorption onto the FeSnSi composite better.

3.14 Comparison of maximum sorption capacity with different composites

The maximum sorption capacity of FeSnSi composite for the sorption of Y(III) and Zr(IV) was compared with other composites reported in the literature. As represented in Table 7, the maximum sorption capacity of FeSnSi is higher than the previously reported values which suggested that this is a promising composites to remove Y(III) and Zr(IV) from aqueous solutions [15–19].

3.15 Binary systems

Figure 8 illustrates the effect of competition on Zr(IV) uptake and separation onto FeSnSi composite at several pHs from the Zr-Y binary system. In the binary system, it is discovered that Zr(IV) has high K_d values at various pHs. Table 8 contains the K_d and α_Y^{Zr} values at various pHs for the binary system. The Zr-Y binary system data showed that K_d had the following sequence: Zr(IV) > Y(III) at all pHs. This sequence supports the idea that Y(III) and Zr(IV) adsorption was accomplished by ionic radii (I.R.) [Y(III) has an I.R. of 0.093 nm, whereas Zr(IV) has an I.R. of 0.08 nm]. Zr(IV) will more readily penetrate the sorbent cavities, increasing sorption and raising K_d [51]. Also, the data reflect that Zr(IV) is high α_Y^{Zr} at different pHs. These findings demonstrate that at various pHs, Zr(IV) can be readily sorbed from the Zr-Y system onto FeSnSi composite.

4 Conclusion

In this work, the batch sorption of Zr(IV) and Y(III) from an aqueous solution using a FeSnSi composite prepared by the co-precipitation method. The sorption of Zr(IV) and Y(III) demonstrates that the FeSnSi composite obeys the PSO kinetic model and has an equilibrium time of 90 min. The thermodynamic functions reflected that the sorption process is endothermic and spontaneous. The applicability of the Langmuir model with the maximum sorption capacity was 34.8 and 41.3 mg g^{-1} for Y(III) and Zr(IV), respectively. According to binary system data, Zr(IV) can be separated from Zr-Y onto FeSnSi composite at different pHs. The previously mentioned data demonstrates that the FeSnSi composite is a material with great potential for the sorption and extraction of Zr(IV) and Y(III) from aqueous solutions.

Fig. 8 Sorption and separation of Zr(IV) from Zr-Y binary system onto FeSnSi composite

Declarations

Ethical approval Is not applicable.

Competing interests The authors declare no competing interests.

References

1. Iftekhar, S., Srivastava, V., Casas, A., et al.: Synthesis of novel GA-g-PAM/SiO$_2$ nanocomposite for the recovery of rare earth elements (REE) ions from aqueous solution. J. Clean. Prod. **170**, 251–259 (2018)

2. Hu, Y., Florek, J., Larivière, D., et al.: Recent advances in the separation of rare earth elements using mesoporous hybrid materials. Chem. Rec. **18**, 1261–1276 (2018)

3. Ryu, S., Fonseka, C., Naidu, G., et al.: Recovery of rare earth elements (Lu, Y) by adsorption using functionalized SBA-15 and MIL-101 (Cr). Chemosphere **281**, 130869 (2021)

4. Huang, Z., Fan, M., Tiand, H.: Coal and coal byproducts: A large and developable unconventional resource for critical materials–Rare earth elements. J. Rare Earths **36**, 337–338 (2018)

5. Dutta, T., Kim, K.-H., Uchimiya, M., et al.: Global demand for rare earth resources and strategies for green mining. Environ. Res. **150**, 182–190 (2016)

6. Rim, K.T., Koo, K.H., Park, J.S.: Toxicological evaluations of rare earths and their health impacts to workers: a literature review. Saf. Health Work **4**, 12–26 (2013)

7. Shin, S.-H., Kim, H.-O., Rim, K.-T.: Worker safety in the rare earth elements recycling process from the review of toxicity and issues. Saf. Health Work **10**, 409–419 (2019)

8. Pagano, G., Guida, M., Tommasi, F., et al.: Health effects and toxicity mechanisms of rare earth elements—Knowledge gaps and research prospects. Ecotoxicol. Environ. Saf. **115**, 40–48 (2015)

9. Shahnaz, T., Priyan, V.V., Jayakumar, A., et al.: Magnetic nanocellulose from Cyperus rotundas grass in the absorptive removal of rare earth element cerium(III): Toxicity studies and interpretation. Chemosphere **287**, 131912 (2022)

10. Hamed, M.M., Rizk, H.E., Ahmed, I.M.: Adsorption behavior of zirconium and molybdenum from nitric acid medium using low-cost adsorbent. J. Mol. Liq. **249**, 361–370 (2018)

11. Atia, A.A., Donia, A.M., Awed, H.A.: Synthesis of magnetic chelating resins functionalized with tetraethylenepentamine for adsorption of molybdate anions from aqueous solutions. J. Hazard. Mater. **155**, 100–108 (2008)

12. Mahrous, S.S., Abass, M.R., Mansy, M.S.: Bentonite phosphate modified with nickel: Preparation, characterization, and application in the removal of ^{137}Cs and $^{152+154}$Eu. Appl. Radiat. Isot. **190**, 110445 (2022)

13. Mansy, M.S., Eid, M.A., Breky, M.M.E., et al.: Sorption behavior of ^{137}Cs, $^{152+154}$Eu and ^{131}Ba from aqueous solutions using inorganic sorbent loaded on talc. J. Radioanal. Nucl. Chem. **332**, 2971–2987 (2023)

14. Oladoja, N.A., Ololade, I.A., Alimi, O.A., et al.: Iron incorporated rice husk silica as a sorbent for hexavalent chromium attenuation in aqueous system. Chem. Eng. Res. Des. **91**, 2691–2702 (2013)

15. Cheira, M.F., Kouraim, M.N., Zidan, I.H., et al.: Adsorption of U(VI) from sulfate solution using montmorillonite/polyamide and nano-titanium oxide/polyamide nanocomposites. J. Environ. Chem. Eng. **8**, 104427 (2020)

16. Bai, R., Yang, F., Meng, L., et al.: Polyethylenimine functionalized and scaffolded graphene aerogel and the application in the highly selective separation of thorium from rare earth. Mater. Des. **197**, 109195 (2021)

17. Faghihian, H., Kabiri-Tadi, M.: Removal of zirconium from aqueous solution by modified clinoptilolite. J. Hazard. Mater. **178**, 66–73 (2010)

18. Mekawy, Z.A., El Shazly, E.A.A., Mahmoud, M.R.: Utilization of bentonite as a low-cost adsorbent for removal of ^{95}Zr(IV), ^{181}Hf(IV) and ^{95}Nb(V) radionuclides from aqueous solutions. J. Radioanal. Nucl. Chem. **331**, 3935–3948 (2022)

19. Zolfonoun, E., Monji, A.B., Taghizadeh, M., et al.: Selective and direct sorption of zirconium from acidic leach liquor of zircon concentrate by rice bran. Miner. Eng. **23**, 755–756 (2010)

20. Ibrahim, A.B., Abass, M.R., EL-Masry, E.H., et al.: Gamma radiation-induced polymerization of polyacrylic acid-dolomite composite and applications for removal of cesium, cobalt, and zirconium from aqueous solutions. Appl. Radiat. Isot. **178**, 109956 (2021)

21. Abass, M.R., Kandeel, E.M., Abou-Lilah, R.A., et al.: Effective biosorption of cesium and strontium ions from aqueous solutions using silica loaded with aspergillus brasiliensis. Water Air Soil Pollut. **235**, 61 (2024)

22. Abass, M.R., Abou-Lilah, R.A., Abou-Mesalam, M.M.: Selective separation of cobalt ions from some fission products using synthesized inorganic sorbent. J. Inorg. Organomet. Polym. Mater. 1–14 (2024)

23. Gupta, V.K., Sharma, G., Pathania, D., et al.: Nanocomposite pectin Zr(IV) selenotungstophosphate for adsorptional/photocatalytic remediation of methylene blue and malachite green dyes from aqueous system. J. Ind. Eng. Chem. **21**, 957–964 (2015)

24. Metwally, S.S., Hassan, H.S., Samy, N.M.: Impact of environmental conditions on the sorption behavior of ^{60}Co and $^{152+154}$Eu radionuclides onto polyaniline/zirconium aluminate composite. J. Mol. Liq. **287**, 110941 (2019)

25. Abass, M.R., Ibrahim, A.B., El-Masry, E.H., et al.: Optical properties enhancement for polyacrylonitrile-ball clay nanocomposite by heavy metals saturation technique. J. Radioanal. Nucl. Chem. **329**, 849–855 (2021)

26. Hamed, M.M., Shahr El-Din, A.M., Abdel-Galil, E.A.: Nanocomposite of polyaniline functionalized Tafla: synthesis, characterization, and application as a novel sorbent for selective removal of Fe(III). J. Radioanal. Nucl. Chem. **322**, 663–676 (2019)

27. Lagergren, S.: Zur theorie der sogenannten adsorption geloster stoffe. K Sven Vetenskapsakademiens Handl. **24**, 1–39 (1898)

28. Ho, Y.S., McKay, G.: The kinetics of sorption of divalent metal ions onto sphagnum moss peat. Water Res. **34**, 735–742 (2000)

29. Abdel-Galil, E.A., Ibrahim, A.B., Abou-Mesalam, M.M.: Sorption behavior of some lanthanides on polyacrylamide stannic molybdophosphate as organic-inorganic composite. Int J Ind Chem. **7**, 231–240 (2016)

30. Şenol, Z.M., Şimşek, S.: Insights into effective adsorption of lead ions from aqueous solutions by using chitosan-bentonite composite beads. J. Polym. Environ. **30**, 3677–3687 (2022)

31. Dakroury, G.A., El-Shazly, E.A.A., Hassan, H.S.: Preparation and characterization of ZnO/Chitosan nanocomposite for Cs(I) and Sr(II) sorption from aqueous solutions. J. Radioanal. Nucl. Chem. **330**, 159–174 (2021)

32. Langmuir, I.: The adsorption of gases on plane surfaces of glass, mica and platinum. J. Am. Chem. Soc. **40**, 1361–1403 (1918)

33. Freundlich, H.: Über die adsorption in lösungen. Zeitschrift Phys. Chem. **57**, 385–470 (1907)

34. Ahmed, I.M., Aglan, R.F., Hamed, M.M.: Removal of Arsenazo-III and Thorin from radioactive waste solutions by adsorption onto low-cost adsorbent. J. Radioanal. Nucl. Chem. **314**, 2253–2262 (2017)

35. Jafari, V., Allahverdi, A.: Synthesis of nanosilica from silica fume using an acid-base precipitation technique and PVA as a nonionic surfactant. J Ultrafine Grained Nanostructured Mater. **47**, 105–112 (2014)

36. Zulfiqar, U., Subhani, T., Wilayat, H.S.: Synthesis of silica nanoparticles from sodium silicate under alkaline conditions. J. Sol-Gel Sci. Technol. **77**, 753–758 (2016)

37. Taufik, A., Saleh, R.: Synthesis of iron (II, III) oxide/zinc oxide/copper (II) oxide (Fe_3O_4/ZnO/CuO) nanocomposites and their photosonocatalytic property for organic dye removal. J. Colloid Interface Sci. **491**, 27–36 (2017)

38. Ahmad, M., Islam, I.U., Ahmad, M., et al.: Preparation of iron-modified biochar from rice straw and its application for the removal of lead (Pb^{+2}) from lead-contaminated water by adsorption. Chem. Pap. **76**, 3789–3808 (2022)

39. Abdel-Galil, E.A., Eid, M.A., Hassan, R.S.: Preparation of nano-sized stannic silicomolybdate for chromatographic separation of Y(III) from Zr(IV). Part. Sci. Technol. **38**, 113–120 (2020)

40. Abass, M.R., Maree, R.M., Sami, N.M.: Adsorptive features of cesium and strontium ions on zirconium tin(IV) phosphate nanocomposite from aqueous solutions. Int. J. Environ. Anal. Chem. **104**, 103–122 (2024)

41. Yakout, S.M., Hassan, H.S.: Adsorption characteristics of sol gel-derived zirconia for cesium ions from aqueous solutions. Molecules **19**, 9160–9172 (2014)

42. Abou-Mesalam, M.M., Abass, M.R., Abdel-Wahab, M.A., et al.: Complex doping of d-block elements cobalt, nickel, and cadmium in magneso-silicate composite and its use in the treatment of aqueous waste. Desalin. Water Treat. **57**, 25757–25764 (2016)

43. Abass, M.R., Ibrahim, A.B., Abou-Mesalam, M.M.: Retention and selectivity behavior of some lanthanides using bentonite dolomite as a natural material. Chem. Pap. **75**, 3751–3759 (2021)

44. Abou-Mesalam, M.M., Abass, M.R., Zakaria, E.S., et al.: Metal doping silicates as inorganic ion exchange materials for environmental remediation. Silicon **14**, 7961–7969 (2022)

45. Taha, K.K., Suleiman, T.M., Musa, M.A.: Performance of Sudanese activated bentonite in bleaching cottonseed oil. J. Bangladesh Chem. Soc. **24**, 191–201 (2011)

46. Nilchi, A., Maalek, B., Khanchi, A., et al.: Cerium(IV) molybdate cation exchanger: synthesis, properties and ion separation capabilities. Radiat. Phys. Chem. **75**, 301–308 (2006)

47. Nabi, S.A., Khan, A.M.: Synthesis, ion exchange properties and analytical applications of stannic silicomolybdate: Effect of temperature on distribution coefficients of metal ions. React. Funct. Polym. **66**, 495–508 (2006)

48. Abdel-Galil, E.A., Ibrahim, A.B., El-Kenany, W.M.: Facile fabrication of a novel silico vanadate ion exchanger: evaluation of its sorption behavior towards europium and terbium ions. Desalin. Water Treat. **226**, 303–318 (2021)

49. Şenol, Z.M., Kaya, S., Şimşek, S., et al.: Synthesis and characterization of chitosan-vermiculite-lignin ternary composite as an adsorbent for effective removal of uranyl ions from aqueous solution: Experimental and theoretical analyses. Int. J. Biol. Macromol. **209**, 1234–1247 (2022)

50. Hamed, M.M., Holiel, M., Ismail, Z.H.: Removal of [134]Cs and [152+154]Eu from liquid radioactive waste using Dowex HCR-S/S. Radiochim. Acta **104**, 399–413 (2016)

51. Abass, M.R., Ibrahim, A.B., Abou-Mesalam, M.M.: Comparative studies for natural and synthetic composites based on molybdate for gadolinium ions separation. Int. J. Environ. Anal. Chem. 1–20 (2022)